Solid gas and electrochemical hydrogenation of the selected alloys (R',R")2-Mg Ni4-Co (R', R" = Pr, Nd; x = 0.8–1.2; y = 0–2)

Yuriy Verbovytskyy, Volodymyr Oprysk, Valérie Paul-boncour, Ihor Zavaliy, Vasyl Berezovets, Pavlo Lyutyy, Yuriy Kosarchyn

Solid gas and electrochemical hydrogenation of the selected alloys $(R',R'')_{2-x}Mg_xNi_{4-y}Co_y$ (R', R'' = Pr, Nd; x = 0.8 - 1.2; y = 0 - 2)

Yuriy Verbovytskyy, Volodymyr Oprysk, Valérie Paul-Boncour, Ihor Zavaliy, Vasyl Berezovets, Pavlo Lyutyy, Yuriy Kosarchyn

Karpenko Physico-Mechanical Institute, NAS of Ukraine, 5 Naukova Str, 79060, Lviv, Ukraine
Université Paris-Est Creteil, CNRS, ICMPE, UMR 7182, F-94320 Thiais, France

Abstract

A number of alloys with the $(R', R'')_{2-x}Mg_xNi_{4-y}Co_y$ (R', R'' = Pr, Nd; x = 0.8 - 1.2; y = 0 - 2) compositions were synthesized by the sintering method and characterized by X-ray powder diffraction method. They are all with cubic $MgCu_4Sn$ structure and belong to the continuous solid solution. Gas hydrogenation was performed for the selected alloys and 15 new hydrides belonging to cubic or orthorhombic structures were obtained. PCT diagrams are constructed for the $Nd_{1.2}Mg_{0.8}Ni_3Co$ - H_2 and $Nd_{0.8}Mg_{1.2}Ni_3Co$ - H_2 systems. The influence of R/Mg and Ni/Co substitution on the discharge characteristics of the $(R', R'')_{2-x}Mg_xNi_{4-y}Co_y$ electrodes was studied. It was established that cobalt-doped alloys with high magnesium content show the highest discharge capacities.

Keywords: rare earth and magnesium alloys, hydrides, electrochemical properties.

1. Introduction

Intensive development of portable devices, in particular electronics, requires the improvement of their power supplies, and among them the rechargeable batteries are frequently used. Nickel-metal hydride (Ni-MH) batteries have attracted considerable attention of researchers for many years. This type of batteries is characterized by high energy consumption, good cyclical stability, environmental friendliness and low cost. Ni-MH batteries are widely used in portable electronics and other fields of technology, such as batteries for hybrid electric vehicles.

Intermetallics, which are able to reversibly absorb hydrogen, are used as negative electrodes for commercial Ni-MH batteries. The alloys of the RM_5 type (R - rare earth metal or their mixture, M - *d*-transition metal) have a discharge capacity of ~300 mAh/g [1-4]. During last decades the Mg-containing alloys and intermetallic phases with general compositions of alloys $R'M_2$, $R'M_3$, R'_2M_7 (R' - mixture of rare earth metals with magnesium, M - *d*-transition metal or their mixture) as potential hydrogen storage materials attract special attention of researchers. This is due to their high reversible hydrogen absorption capacity, simple and/or with one stage preparation by various methods and the cheapness of raw materials, which is especially important for practical application [5].

Intermetallic compounds of the $RMgM_4$ (1:1:4) composition and alloys based on them have been intensively studied during the last ten years [6]. They are interesting not only in a view of their structural features and physical properties, but also of their hydrogen sorption properties [7]. Most of these alloys reversibly absorb hydrogen from the gas phase and electrochemically. The amount of absorbed hydrogen can reach up to 6 H/f.u. The maximum discharge capacity of 400 mAh/g is established by the authors [8]. Although there are many studies on the hydrogen adsorption properties of the $RMgM_4$ containing alloys [9], a comprehensive study of the single-phase $RMgM_4$ samples is limited to a few dozen works, most of which are devoted to the study of stoichiometric compositions [10-18].

Recently, we conducted a detailed study of several 1:1:4 alloy systems and have shown the element substitution effects on structural, hydrogen sorption and electrochemical properties [19-25]. In some cases the characteristics of the alloys were improved. In the present paper we report new

data on the synthesis, structural, hydrogen storage and electrochemical properties of the (R', R'')$_{2-x}$Mg$_x$Ni$_{4-y}$Co$_y$ (R', R'' = Pr, Nd; x = 0.8 - 1.2; y = 0 - 2) alloys.

2. Experimental details

The alloys were prepared by sintering method using powdered ingredients. We used rare earth and transition metals and magnesium powder with purity more than 99.8%. At the beginning, alloy (R',R'')(Ni,Co)$_2$ precursors were prepared by arc melting in purified argon atmosphere. Further obtained buttons were ground to the size less than 0.08 mm, mixed with 325 mesh Mg in appropriate proportion and pressed into pellets at 10 ton/cm^2. Magnesium was added with 3 wt % excess to compensate for its evaporation loss at high temperatures. Total weight of each sample was 2-3 grams. Finally, samples were further heated up to 800 °C and down to 500 °C within one week, and annealed at 500 ºC three weeks.

Structural analysis of the samples was carried out by X-ray powder diffraction (XRD) using a DROM 3M diffractometer (Cu Kα radiation). Phase analysis and crystal structures refinement were conducted with a help of PowderCell [26], FullProf [27] and WinCSD [28] programs. Elemental composition of the alloys was examined by scanning electron microscopy (SEM) using an EVO 40XVP microscope equipped with Inca Energy 350 spectrometer for energy dispersive X-ray analysis (EDX).

Hydrogen absorption-desorption properties of the alloys were characterized using a Sieverts-type apparatus. The samples were activated by heating up to 300 °C in dynamic vacuum, cooled to room temperature, and then hydrogenated with high-purity hydrogen gas (99.999 %).

The electrode materials were prepared by mixing powdered alloys with carbonyl Ni powder (1:3). The pellet electrode was made by cold-pressing the powder mixture into a pellet under a pressure of 10 ton/cm^2 and then sandwiched between two Ni foams with fixed conductor. Electrochemical properties were tested in a three-electrode system. Platinum auxiliary and metal hydride (MH) working electrodes were placed in a glass cell with filled 6 M KOH solution electrolyte, while the silver-chloride reference electrode was connected to the system via an agar bridge. Cycling stability of the MH electrodes was studied galvanostatically at a current density of 50 and 200 mA/g at room temperature. The end potential of the discharge was set at 0.6 V vs. the Ag/AgCl electrode.

3. Results and discussion

3.1. Crystal structure of parent alloys

A series of the (R', R'')$_{2-x}$Mg$_x$Ni$_{4-y}$Co$_y$ (R', R'' = Pr, Nd; x = 0.8 - 1.2; y = 0 - 2) alloys were synthesized by sintering method. According to the results of X-ray phase analysis, all samples were single-phase and belong to the SnMgCu$_4$ structural type (space group *F-43m*). In the structure of stoichiometric composition RMgM$_4$, rare earth metal atoms occupy the position of Mg atoms (4*a*), Mg atoms are located in the Sn sites (4*c*), and transition metal atoms distribute the Cu positions (16*e*). In the structure of phases (Pr$_{0.5}$Nd$_{0.5}$)$_{2-x}$Mg$_x$Ni$_{4-y}$Co$_y$, where x ≠ 1, the atoms R and Mg form statistical mixtures and occupy the (4*a*) and/or (4*c*) sites. Additionally, the sample with the highest cobalt content, namely, Pr$_{0.5}$Nd$_{0.5}$MgNiCo$_3$, contained also only one cubic phase (a = 7.1361 (7) Å, V = 363.39(6) Å^3). All above mentioned phases belong to continuous solid solutions showing widely varying ratio of R/Mg and Ni/Co atoms. The refined lattice parameters of the studied alloys are presented in Table. 1. For comparison, crystallographic data of previously studied alloys are also given in Table 1. As the radii of rare earth atoms and magnesium increase from Mg to Pr/Nd as well as transition atoms from Ni to Co, the lattice parameters increase gradually upon substitution. Refined X-ray diffraction patterns of selected alloys are illustrated in Fig. 1.

Table 1. Calculated lattice parameters of the parent alloys

x_{Mg}	y_{Co}			
	0	0.5	1	2
0.8	-	-	$Pr_{1.2}Mg_{0.8}Ni_3Co$ 7.1437(4)	-
0.8	-	$Pr_{0.6}Nd_{0.6}Mg_{0.8}Ni_{3.5}Co_{0.5}$ 7.1336(5)	$Pr_{0.6}Nd_{0.6}Mg_{0.8}Ni_3Co$ 7.1371(5)	-
0.8	$Nd_{1.2}Mg_{0.8}Ni_4$ 7.1108(4)	-	$Nd_{1.2}Mg_{0.8}Ni_3Co$ 7.1316(3)	-
1.0	$PrMgNi_4$ 7.1098(2) [21]	$PrMgNi_{3.5}Co_{0.5}$ 7.1162(2) [21]	$PrMgNi_3Co$ 7.1200(2) [21]	$PrMgNi_2Co_2$ 7.1269(3) [21]
1.0	$Pr_{0.5}Nd_{0.5}MgNi_4$ 7.1054(2)	$Pr_{0.5}Nd_{0.5}MgNi_{3.5}Co_{0.5}$ 7.1103(3)	$Pr_{0.5}Nd_{0.5}MgNi_3Co$ 7.1189(3)	$Pr_{0.5}Nd_{0.5}MgNi_2Co_2$ 7.1198(4)
1.0	$NdMgNi_4$ 7.0923(4) [22]	$NdMgNi_{3.5}Co_{0.5}$ 7.1010(4) [22]	$NdMgNi_3Co$ 7.1046(2) [22]	$NdMgNi_2Co_2$ 7.1184(1) [22]
1.2	-	-	$Pr_{0.8}Mg_{1.2}Ni_3Co$ 7.0652(4)	-
1.2	$Pr_{0.4}Nd_{0.4}Mg_{1.2}Ni_4$ 7.0501(6)	$Pr_{0.4}Nd_{0.4}Mg_{1.2}Ni_{3.5}Co_{0.5}$ 7.0551(5)	$Pr_{0.4}Nd_{0.4}Mg_{1.2}Ni_3Co$ 7.0615(5)	$Pr_{0.4}Nd_{0.4}Mg_{1.2}Ni_2Co_2$ 7.0700(7)
1.2	$Nd_{0.8}Mg_{1.2}Ni_4$ 7.0472(6)	-	$Nd_{0.8}Mg_{1.2}Ni_3Co$ 7.0510(4)	-

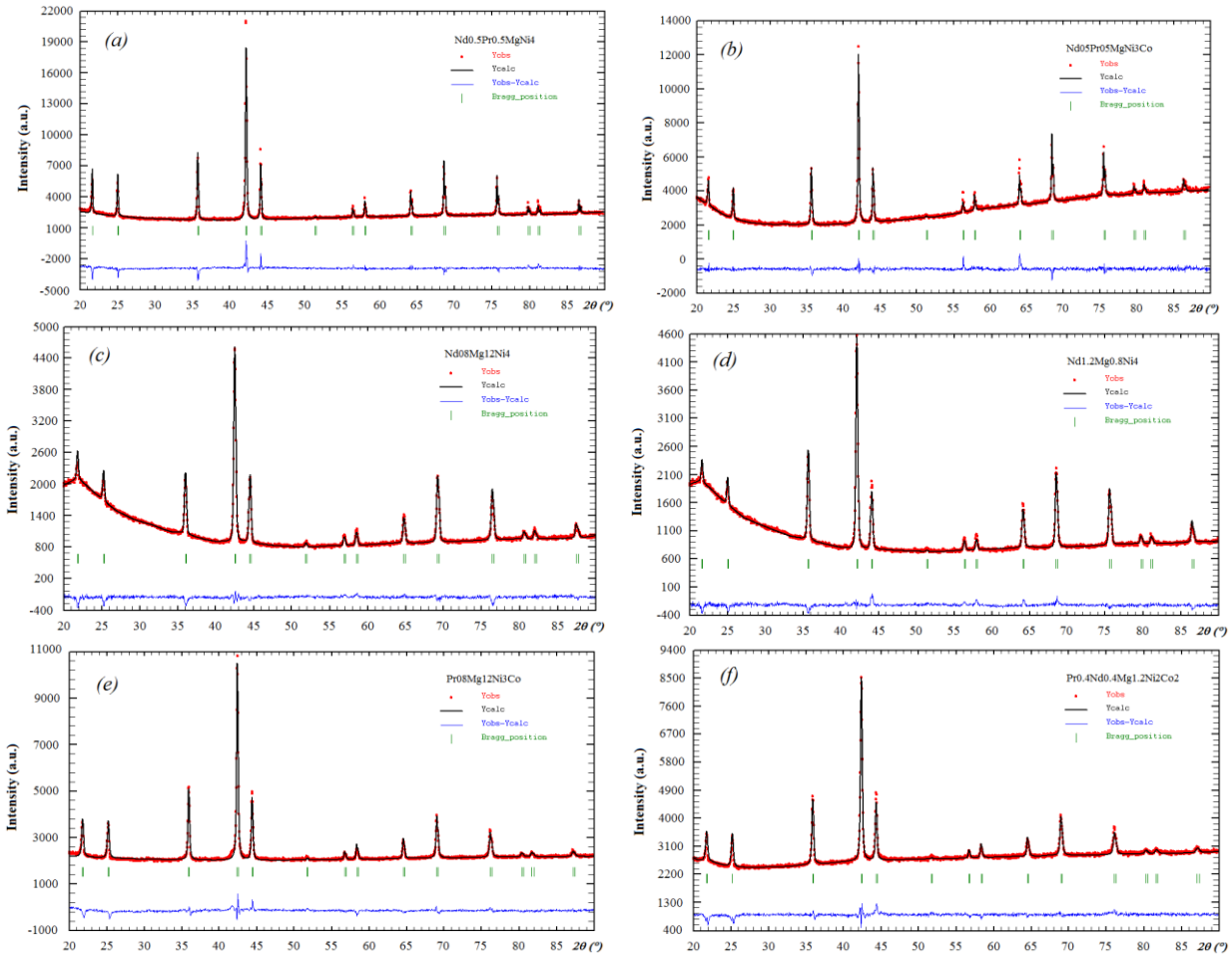

Fig. 1. Rietveld refinements of the XRD patterns for: (*a*) $Pr_{0.5}Nd_{0.5}MgNi_4$; (*b*) $Pr_{0.5}Nd_{0.5}MgNiCo_3$, (*c*) $Nd_{0.8}Mg_{1.2}Ni_4$, (*d*) $Nd_{1.2}Mg_{0.8}Ni_4$, (*e*) $Pr_{0.8}Mg_{1.2}Ni_3Co$, (*f*) $Pr_{0.4}Nd_{0.4}Mg_{1.2}Ni_2Co_2$.

All samples were analyzed by semiquantitative EDX analysis with internal standards. Surfaces of the selected alloys are shown in Fig. 2. Measured compositions of the alloys are close to the nominal ones for the majority of the compounds. The experimentally observed compositions were all within ±0.1-0.5 at. %. No impurities were observed.

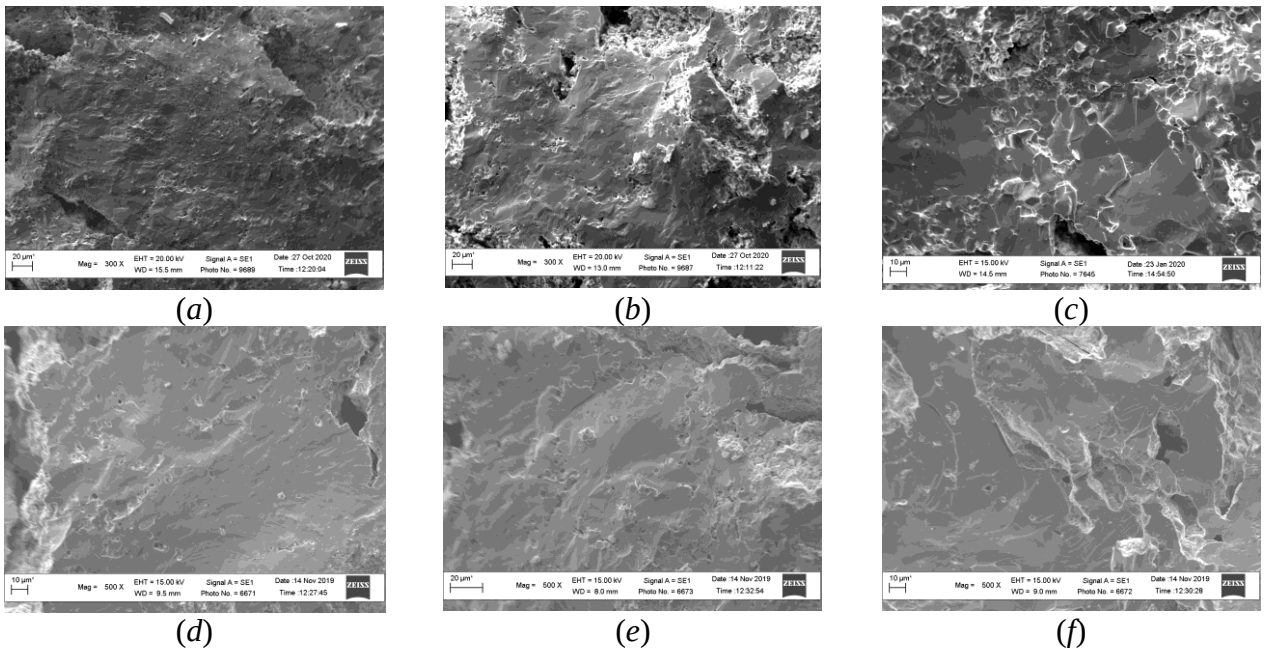

Fig. 2. Microphotographs of the surface of the selected alloys:
(*a*) $Nd_{1.2}Mg_{0.8}Ni_4$, (*b*) $Nd_{0.8}Mg_{1.2}Ni_4$, (*c*) $Pr_{0.6}Nd_{0.6}Mg_{0.8}Ni_{3.5}Co_{0.5}$,
(*d*) $Nd_{1.2}Mg_{0.8}Ni_3Co$, (*e*) $Pr_{0.6}Nd_{0.6}Mg_{0.8}Ni_3Co$, (*f*) $Nd_{0.8}Mg_{1.2}Ni_3Co$.

3.2. Solid-gas hydrogenation

Selected alloys were crushed into small pieces and hydrogenated. The alloys easily absorb hydrogen at room temperature and maximum pressure up to 13 bar. Curves of the first hydrogenation are presented in Fig. 3. All investigated alloys have an incubation period not exceeding 30 minutes. Then there is a period corresponding to the active hydrogen absorption, which ends with slow absorption and final saturation. Experimental data were further analyzed using the Johnson-Mehl-Avrami equation: $y = 1 - \exp[-(k \cdot x)^n]$, where y is the completeness of the reaction or the volume fraction of unreacted material ($0 < y < 1$), x is the reaction time (min), k is the reaction rate constant (min^{-1}), n is the kinetic parameter (indicating the reaction mechanism). The kinetic characteristics obtained by using this equation are shown in Table 2. The value of the exponent n can be used to judge the conditions of formation and growth of nuclei, and reaction mechanism. Here $n > 1$, thus the reaction rate depends weakly on the rate of nucleation and it is determined mainly by the growth of existing nuclei.

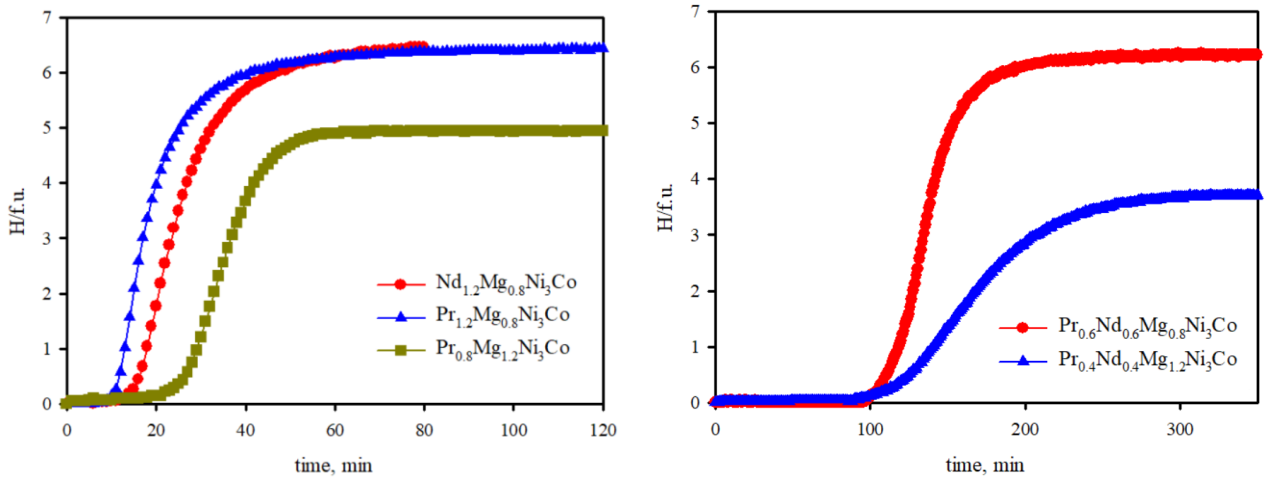

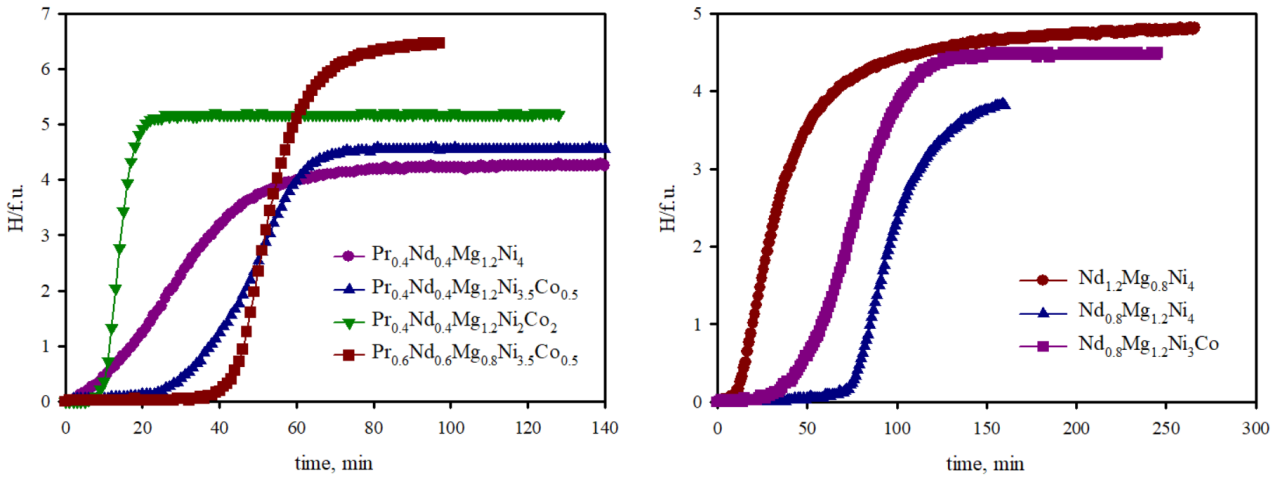

Fig. 3. Curves of first hydrogenation cycle of the selected alloys

Table. 2. Hydrogenation conditions and values of the reaction rate constants according JMA equation

№	Alloy	*P, bar*	H/M	H wt.%	*k*	*n*	R^2
1.	$Nd_{1.2}Mg_{0.8}Ni_3Co$	7.20	6.44	1.50	0.0347(3)	2.99(11)	0.989
2.	$Pr_{1.2}Mg_{0.8}Ni_3Co$	4.91	6.43	1.51	0.0455(5)	2.53(9)	0.986
3.	$Pr_{0.8}Mg_{1.2}Ni_3Co$	9.30	4.98	1.31	0.0263(1)	5.06(6)	0.998
4.	$Pr_{0.4}Nd_{0.4}Mg_{1.2}Ni_4$	12.57	4.31	1.14	0.0285(1)	1.84(1)	0.999
5.	$Pr_{0.4}Nd_{0.4}Mg_{1.2}Ni_{3.5}Co_{0.5}$	8.85	4.55	1.20	0.0193(1)	4.59(2)	0.999
6.	$Pr_{0.4}Nd_{0.4}Mg_{1.2}Ni_3Co$	3.51	3.67	0.97	0.05503(1)	4.40(4)	0.997
7.	$Pr_{0.4}Nd_{0.4}Mg_{1.2}Ni_2Co_2$	7.90	5.17	1.36	0.0666(2)	5.29(9)	0.999
8.	$Pr_{0.6}Nd_{0.6}Mg_{0.8}Ni_{3.5}Co_{0.5}$	8.83	6.46	1.51	0.0178(1)	7.46(23)	0.995
9.	$Pr_{0.6}Nd_{0.6}Mg_{0.8}Ni_3Co$	3.46	6.21	1.45	0.00692(1)	7.87(12)	0.997
10.	$Nd_{1.2}Mg_{0.8}Ni_4$	10.28	4.80	1.12	0.0221(1)	1.44(2)	0.994
11.	$Nd_{0.8}Mg_{1.2}Ni_4$	5.17	3.81	1.00	0.0096(1)	5.86(13)	0.992
12.	$Nd_{0.8}Mg_{1.2}Ni_3Co$	5.53	4.48	1.18	0.01200(1)	3.68(2)	0.999

Isotherms of hydrogen absorption and desorption for the $Nd_{1.2}Mg_{0.8}Ni_3Co$ - H_2 and $Nd_{0.8}Mg_{1.2}Ni_3Co$ - H_2 systems were obtained at 25, 50, 75 and/or 80 °C up to 10 bar and are shown in Fig. 4. As can be seen in this figure, for Mg contents 0.8 and 1.2 a fully reversible hydrogenation takes place with the single plateau pressure observed in the isotherms between the alloys and the hydrides. This plateau displays a slope for $Nd_{1.2}Mg_{0.8}Ni_3Co$ - H_2 which is not observed for $Nd_{0.8}Mg_{1.2}Ni_3Co$ - H_2. At 10 bar the maximum H/M capacity of $Nd_{1.2}Mg_{0.8}Ni_3Co$ is significantly higher than that of $Nd_{0.8}Mg_{1.2}Ni_3Co$ - H_2. However a very slow kinetics was observed for $Nd_{1.2}Mg_{0.8}Ni_3Co$ at 25°C, the hydride showed high stability, and therefore hydrogen could not be completely desorbed at this temperature due to low pressure. This induces a limited reversible capacity at room temperature. In case of $Nd_{0.8}Mg_{1.2}Ni_3Co$, the hydrogenation kinetic is slightly higher compared to $Nd_{1.2}Mg_{0.8}Ni_3Co$. Lowering of the plateau pressure associated with larger capacities versus Mg content has been recently observed in $Y_{1-x}Mg_xNi_4$ alloys [29].

Thermodynamic parameters of hydride formation and decomposition were calculated from the Van't Hoff plots. The following parameters are obtained: ΔH_{abs} = -46.5 kJ/mol H_2, ΔS_{abs} = -125.9 J/mol H_2 · K and ΔH_{des} = 41.3 kJ/mol H_2, ΔS_{des} = 100.4 J/mol H_2 · K for $Nd_{1.2}Mg_{0.8}Ni_3Co$ and ΔH_{abs} = -43.5 kJ/mol H_2, ΔS_{abs} = -141.1 J/mol H_2 · and ΔH_{des} = 36.8 kJ/mol H_2, ΔS_{des} = 116.3 J/mol H_2 · K K for $Nd_{0.8}Mg_{1.2}Ni_3Co$. The thermodynamic data of the present study show a very significant variation of the values versus the Mg content. Here, we can compare calculated ΔH_{abs} and ΔS_{abs} for investigated alloys with those ones for $PrMgNi_4$ (ΔH_{abs} = -42,4 kJ/mol H_2, ΔS_{abs} = -126,8 J/mol H_2 · K), $Pr_{0.8}Mg_{1.2}Ni_4$ (ΔH_{abs} = -40,3 kJ/mol H_2, ΔS_{abs} = -128,6 J/mol H_2 · K) and $Pr_{0.6}Mg_{1.4}Ni_4$ (ΔH_{abs} = -39,2 kJ/mol H_2, ΔS_{abs} = -133,0 J/mol H_2 · K) [14]. We note that ΔH_{abs} decrease and ΔS_{abs} increase when the magnesium content increase.

3.3. Crystal structure of the hydrides

Fifteen new hydrides were synthesized by direct hydrogenation of the parent alloys. All the obtained hydrides were exposed to air to passivate the surface and were characterized by X-ray diffraction. Rietveld refinements of the selected XRD patterns are illustrated in Fig. 5. Preserved parent cubic structure was detected for almost all hydrides. Only, two hydrides, namely, $Pr_{0.5}Nd_{0.5}MgNi_4H_4$ and $Nd_{1.2}Mg_{0.8}Ni_4H_{4.80}$ were found with orthorhombic structures. Last one was unstable and partially decomposed after synthesis. It should be noted that the $Nd_{1.2}Mg_{0.8}Ni_3CoH_{1.8}$ hydride was prepared by partial hydrogen desorption from a high saturated hydride. The increase of cell volume versus H content confirms the existence of a solid solution for this compound.

As can we see from XRD, the hydrides of the alloys with the lowest magnesium content besides the crystalline phase also contained an amorphous one. This is deduced from the relatively smaller peak intensity for a same counting time. In addition, the XRD patterns of the compounds which contain 0.8 Mg display broader line widths than those with 1 or 1.2 Mg, suggesting smaller crystallite sizes for low Mg content. Volume expansion of the unit cell for saturated hydrides compared to their parent alloys is in the range 13 - 20 %. In general, volume evolution is in good agreement with absorbed quantity of hydrogen. Refined crystallographic parameters of the orthorhombic and cubic hydrides are presented in Table 3.

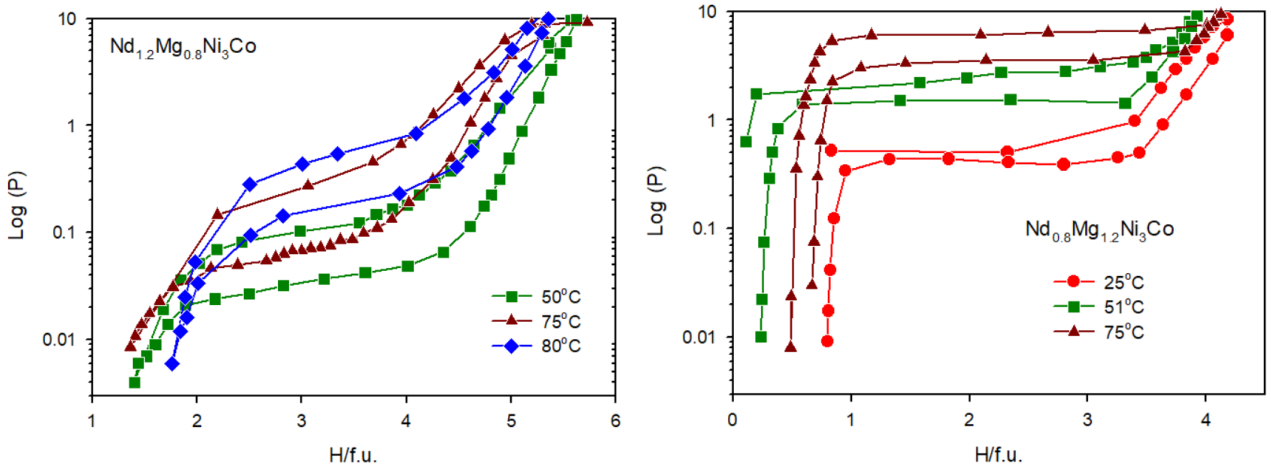

Fig. 4. Absorption-desorption isotherms in the $Nd_{1.2}Mg_{0.8}Ni_3Co$ - H_2 and $Nd_{0.8}Mg_{1.2}Ni_3Co$ - H_2 systems

Table. 3. Calculated lattice parameters of the hydrides

№	Hydride	*a* (Å)	*V* (Å^3)	Δ*V*, %	Δ*V*/*Zn*	Remarks
1.	$Nd_{1.2}Mg_{0.8}Ni_4H_{4.80}$	5.0896(32) 5.5038(35) 7.3872(45)	206.9(2)	15.1	2.83	Partially amorphous, unstable
2.	$Pr_{0.6}Nd_{0.6}Mg_{0.8}Ni_{3.5}Co_{0.5}H_{6.46}$	7.526(11)	426.3(11)	17.4	2.45	Partially amorphous
3.	$Pr_{0.6}Nd_{0.6}Mg_{0.8}Ni_3CoH_{6.21}$	7.576(6)	434.9(6)	19.6	2.87	Partially amorphous
4.	$Pr_{1.2}Mg_{0.8}Ni_3CoH_{6.46}$	7.587(12)	436.8(11)	19.8	2.79	Partially amorphous
5.	$Nd_{1.2}Mg_{0.8}Ni_3CoH_{6.44}$	7.555(6)	431.2(6)	18.9	2.66	Partially amorphous
6.	$Nd_{1.2}Mg_{0.8}Ni_3CoH_{5.8}$	7.514(3)	424.2(3)	17.0	2.65	Partially amorphous
6.	$Nd_{1.2}Mg_{0.8}Ni_3CoH_{1.8}$	7.148(5)	365.2(4)	0.7	0.35	Partially amorphous
7.	$Pr_{0.5}Nd_{0.5}MgNi_4H_{4.0}$	5.087(1) 5.489(1)	206.48(9)	15.1	3.39	Crystalline

		7.395 (2)				
8.	$Pr_{0.5}Nd_{0.5}MgNi_2Co_2H_{6.0}$	7.532 (1)	427.3(1)	18.3	2.76	Crystalline
9.	$Pr_{0.4}Nd_{0.4}Mg_{1.2}Ni_4H_{4.27}$	7.3612(6)	398.89(5)	13.8	2.84	Crystalline
10.	$Nd_{0.8}Mg_{1.2}Ni_4H_{3.81}$	7.3437(5)	396.04(5)	13.2	3.02	Crystalline
11.	$Pr_{0.4}Nd_{0.4}Mg_{1.2}Ni_{3.5}Co_{0.5}H_{4.55}$	7.3718(8)	400.61(8)	14.1	2.72	Crystalline
12.	$Pr_{0.4}Nd_{0.4}Mg_{1.2}Ni_3CoH_{3.67}$	7.3874(4)	403.16(4)	14.5	3.47	Crystalline
13.	$Pr_{0.8}Mg_{1.2}Ni_3CoH_{4.97}$	7.390 (1)	403.6(1)	14.4	2.56	Crystalline
14.	$Nd_{0.8}Mg_{1.2}Ni_3CoH_{4.48}$	7.3701(9)	400.33(9)	14.2	2.78	Crystalline
15.	$Pr_{0.4}Nd_{0.4}Mg_{1.2}Ni_2Co_2H_{5.17}$	7.397(2)	404.7(2)	14.5	2.48	Crystalline

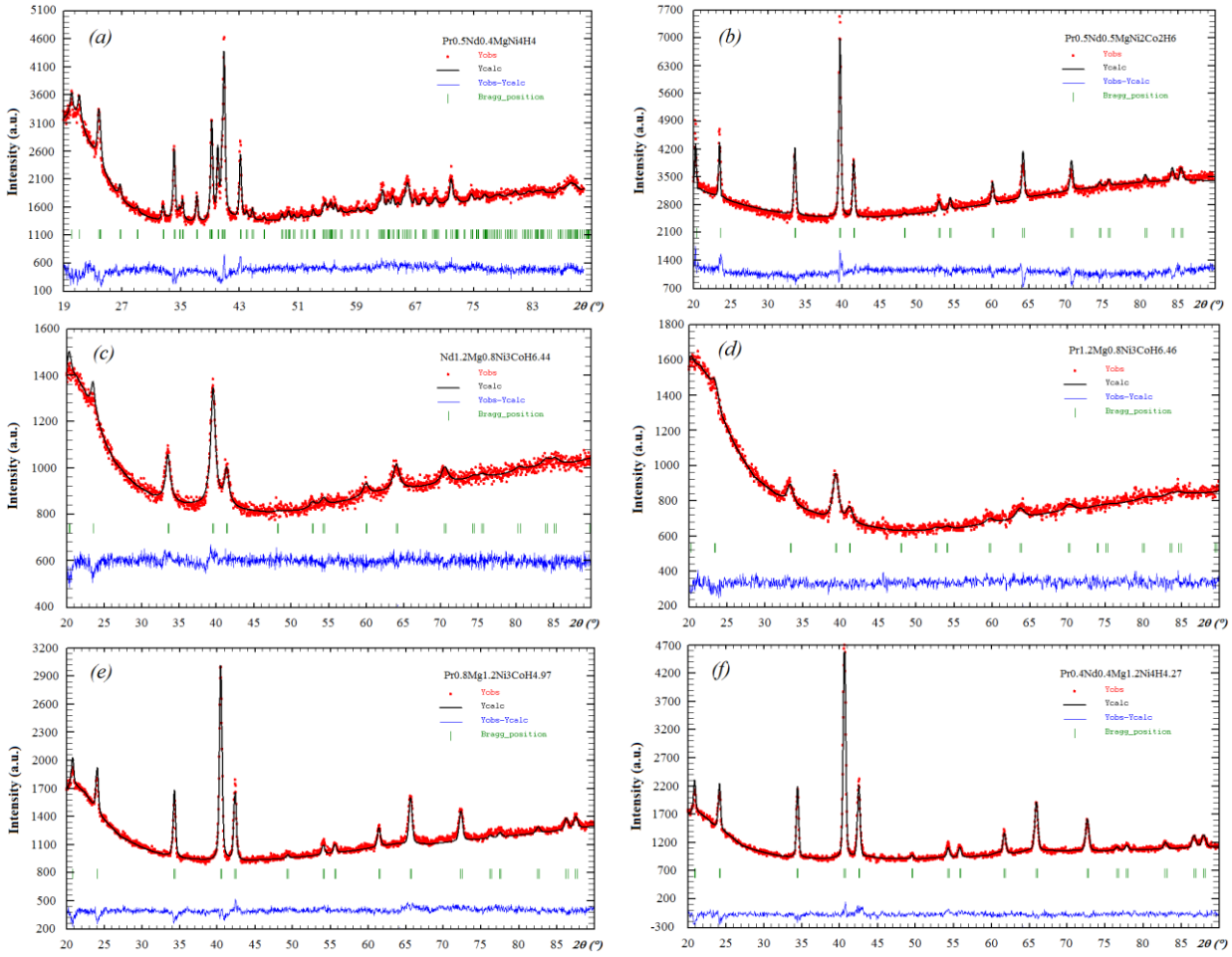

Fig. 5. Rietveld refinements of the XRD patterns for: (*a*) $Pr_{0.5}Nd_{0.5}MgNi_4H_4$; (*b*) $Pr_{0.5}Nd_{0.5}MgNi_2Co_2H_6$, (*c*) $Nd_{1.2}Mg_{0.8}Ni_3CoH_{6.44}$, (*d*) $Pr_{1.2}Mg_{0.8}Ni_3CoH_{6.46}$, (*e*) $Pr_{0.8}Mg_{1.2}Ni_3CoH_{4.97}$, (*f*) $Pr_{0.4}Nd_{0.4}Mg_{1.2}Ni_4H_{4.27}$.

3.4. Electrochemical properties

3.4.1. The $(Pr_{0.5}Nd_{0.5})_{2-x}Mg_xNi_{4-y}Co_y$ (x = 1; y = 0 - 3) alloys

At the beginning the $(Pr_{0.5}Nd_{0.5})_{2-x}Mg_xNi_{4-y}Co_y$ (x = 1; y = 0 - 3) alloys were studies as materials for negative electrodes for Ni-MH batteries at charge/discharge current densities of 50 and 200 mA/g. Maximum discharge capacity of 263 mAh/g (I = 50 mA/g), which corresponds to almost 4 H/f.u., is obtained for the $Pr_{0.5}Nd_{0.5}MgNi_3Co$ electrode. The lowest value of 54 mAh/g (0.8 H/f.u.) is found for the $Pr_{0.5}Nd_{0.5}MgNiCo_3$ electrode, which is the result of high cobalt content in the alloy. To achieve their maximum capacity all electrodes need different number of activation cycles. For example, the $Pr_{0.5}Nd_{0.5}MgNi_4$, $Pr_{0.5}Nd_{0.5}MgNi_{3.5}Co_{0.5}$ and $Pr_{0.5}Nd_{0.5}MgNi_3Co$ electrodes reached maximum capacity after 10-20 cycles, while the $Pr_{0.5}Nd_{0.5}MgNi_2Co_2$ and $Pr_{0.5}Nd_{0.5}MgNiCo_3$ ones – was reached after only 2-3 initial cycles. Discharge capacities as a function of discharge cycle at I = 50 mA/g are presented in Fig. 6 (*a*). After 50 cycles discharge capacity for the $Pr_{0.5}Nd_{0.5}MgNi_2Co_2$ and $Pr_{0.5}Nd_{0.5}MgNi_2Co_2$ electrodes drastically decay to 73 and 32 mAh/g, corresponding to S_{50} = 45

and 60%, respectively. Other Co-poor or Co-free alloy based electrodes demonstrate good stability, with S_{50} varying between 87-90%. Some electrochemical properties are listed in Table 4.

A slightly different trend is observed for samples at a current density of 200 mA/h. The maximum discharge capacity of 188 mAh/g is observed for the $Pr_{0.5}Nd_{0.5}MgNi_{3.5}Co_{0.5}$ electrode, corresponding to less than 3 at. H f.u. The sample with the highest cobalt content shows the lowest discharge capacity - only 25 mAh/g (about 0.4 at. H/f.u.). It should also be noted that at a current density of 200 mA/h the number of cycles required to activate the electrodes increases up to 25 cycles. Discharge capacities as a function of discharge cycle at I = 200 mA/g are displayed in Fig. 6 (*b*). Here, we can also observe the difference of the cyclic stability of the electrodes. The Co-free electrode shows the best stability, as it retains 60% of the maximum capacity after 100 charge-discharge cycles. Other electodes exibhit S_{100} with 51-68% (see Table 5).

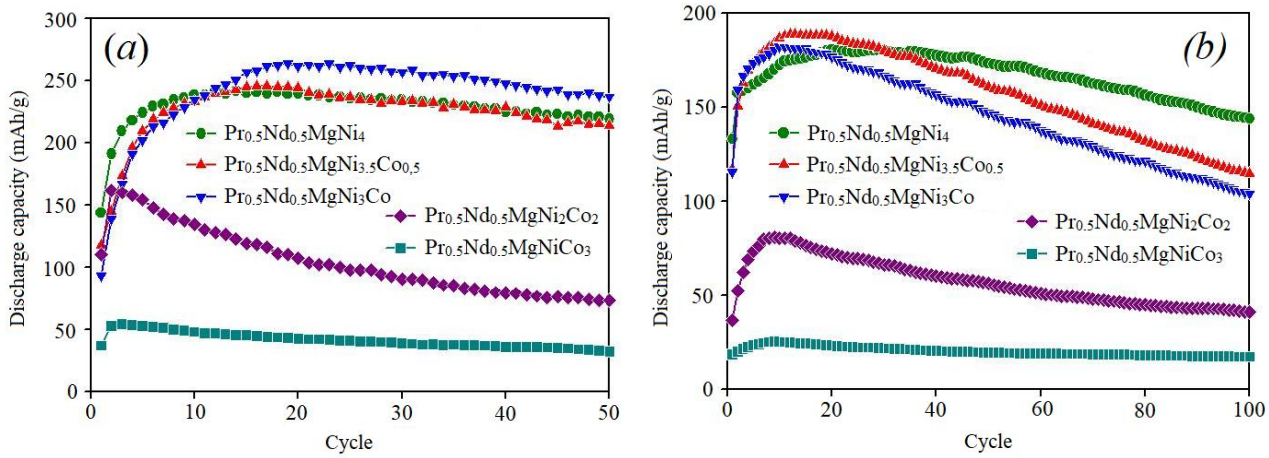

Fig. 6. Cyclic stability of the $Pr_{0.5}Nd_{0.5}MgNi_{4-y}Co_y$ electrodes.
Discharge current density at I = 50 mA/g (*a*) and I = 200 mA/g (*b*).

Table 4. Selected electrochemical properties of the $Pr_{0.5}Nd_{0.5}MgNi_{4-y}Co_y$ electrodes at I = 50 mA/g

№	Electrode	C_{max}, mAh/g	C_{50}, mAh/g	S_{50} (%)	H_{max} / f.u.
1	$Pr_{0.5}Nd_{0.5}MgNi_4$	242	219	90	3.6
2	$Pr_{0.5}Nd_{0.5}MgNi_{3.5}Co_{0.5}$	245	214	87	3.7
3	$Pr_{0.5}Nd_{0.5}MgNi_3Co$	263	237	90	3.9
4	$Pr_{0.5}Nd_{0.5}MgNi_2Co_2$	161	73	45	2.4
5	$Pr_{0.5}Nd_{0.5}MgNiCo_3$	54	32	60	0.8

Table 5. Selected electrochemical properties of the $Pr_{0.5}Nd_{0.5}MgNi_{4-y}Co_y$ electrodes at I = 200 mA/g

№	Electrode	C_{max}, mAh/g	C_{100}, mAh/g	S_{100} (%)	H_{max} / f.u.
1	$Pr_{0.5}Nd_{0.5}MgNi_4$	180	144	80	2.7
2	$Pr_{0.5}Nd_{0.5}MgNi_{3.5}Co_{0.5}$	188	114	61	2.8
3	$Pr_{0.5}Nd_{0.5}MgNi_3Co$	182	104	57	2.7
4	$Pr_{0.5}Nd_{0.5}MgNi_2Co_2$	80	41	51	1.2
5	$Pr_{0.5}Nd_{0.5}MgNiCo_3$	25	17	68	0.4

3.4.2. The $(R',R'')_{2-x}Mg_xNi_{4-y}Co_y$ (R', R'' = Pr, Nd; *x* = 0.8 or 1.2; *y* = 0 - 2) alloys

In this part we analyze the influence of magnesium content and cobalt substitution in the alloys on the electrochemical properties of selected electrodes. Discharge capacities for the electrodes were obtained at a current density of 200 mA/h. Charge-discharge process for each electrode was repeated 50 times. Recorded cyclic stability can be seen in Fig. 7. Summarized electrochemical properties of the studied electrodes are given in Table 6. From the obtained results it can be seen that the electrodes based on alloys with *x* = 1.2 are characterized by average discharge capacities 1.5 - 2.0 times larger than the corresponding ones with *x* = 0.8. The smallest maximum discharge capacity of 160 mAh/g (2.54 at. H f.u.) is detected for the $Pr_{0.6}Nd_{0.6}Mg_{0.8}Ni_3Co$ electrode, and the largest one of 309 mAh/g (4.38 at. H f.u.) is recorded for $Pr_{0.4}Nd_{0.4}Mg_{1.2}Ni_2Co_2$. Maximum discharge capacities of the above mentioned electrodes with *x* = 0.5 have intermediate values. The

influence of the nature of rare earth metals, either the content of single metal (neodymium or praseodymium) or their statistical mixture, on the electrochemical properties is insignificant and almost unchanged for the electrodes with $y = 1$. For the electrodes with $x = 0.5$ cobalt substitution did not lead to significantly improved electrochemical properties, but for the electrodes with $x \neq 1$ the change is clearly visible. For the electrodes with $x = 1.2$, within the series $Pr_{0.4}Nd_{0.4}Mg_{1.2}Ni_4$ - $Pr_{0.4}Nd_{0.4}Mg_{1.2}Ni_{3.5}Co_{0.5}$ - $Pr_{0.4}Nd_{0.4}Mg_{1.2}Ni_3Co$ - $Pr_{0.4}Nd_{0.4}Mg_{1.2}Ni_2Co_2$, maximum discharge capacity increases: 262 - 276 - 293 - 309 mAh/g. The cyclic stability of all studied electrodes is obviously sensitive to many factors and does not show a clear behavior, as it changes from S_{50} = 52% ($Pr_{0.6}Nd_{0.6}Mg_{0.8}Ni_{3.5}Co_{0.5}$) to 80% ($Nd_{0.8}Mg_{1.2}Ni_4$).

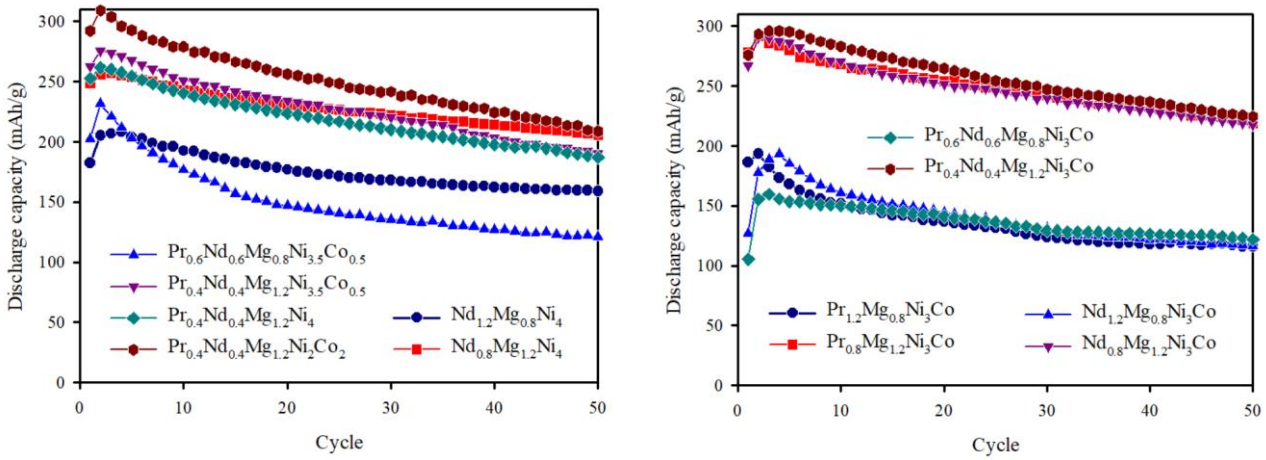

Fig. 7. Cyclic stability of the $(R',R'')_{2-x}Mg_xNi_{4-y}Co_y$ electrodes at I = 50 mA/g.

Table 6. Selected electrochemical properties of the $(R',R'')_{2-x}Mg_xNi_{4-y}Co_y$ ($x \neq 1$) electrodes at I = 50 mA/g

№	Electrode	C_{max}, mAh/g	H_{max} / f.u.	C_{50}, mAh/g	H_{50} / f.u.	S_{50} (%)
1.	$Nd_{1.2}Mg_{0.8}Ni_4$	208	3.32	159	2.54	76
2.	$Nd_{1.2}Mg_{0.8}Ni_3Co$	193	3.08	116	1.85	60
3.	$Pr_{1.2}Mg_{0.8}Ni_3Co$	193	3.06	116	1.84	60
4.	$Pr_{0.6}Nd_{0.6}Mg_{0.8}Ni_{3.5}Co_{0.5}$	232	3.69	121	1.92	52
5.	$Pr_{0.6}Nd_{0.6}Mg_{0.8}Ni_3Co$	160	2.54	122	1.94	76
6.	$Nd_{0.8}Mg_{1.2}Ni_4$	257	3.65	206	2.92	80
7.	$Nd_{0.8}Mg_{1.2}Ni_3Co$	290	4.12	218	3.10	75
8.	$Pr_{0.8}Mg_{1.2}Ni_3Co$	292	4.12	219	3.09	75
9.	$Pr_{0.4}Nd_{0.4}Mg_{1.2}Ni_4$	262	3.71	187	2.65	71
10.	$Pr_{0.4}Nd_{0.4}Mg_{1.2}Ni_{3.5}Co_{0.5}$	276	3.91	190	2.69	69
11.	$Pr_{0.4}Nd_{0.4}Mg_{1.2}Ni_3Co$	293	4.19	224	3.17	76
12.	$Pr_{0.4}Nd_{0.4}Mg_{1.2}Ni_2Co_2$	309	4.38	209	2.96	68

3.4.3. Discussion on electrochemical properties

It is well known that intermetallic phases and alloys effectively work as electrode materials in the Ni-MH batteries when their equilibrium plateau according to PCT is located in the so-called electrochemical window, which is conditionally limited by a pressure of 0.01 - 1 bar. Outside of this range electrode materials already exhibit lower discharge capacities and less interesting from a practical point of view. In our previous works [20, 22], we have shown that the substitution of cobalt for nickel significantly increases hydrogen sorption capacity of the alloys and yields the formation of cubic hydrides with high hydrogen content up to 6.5 H/f.u. The right part of curves of the PCT diagrams for the cobalt containing alloys have sloping shape, which indicates on the hydride formation with variable hydrogen content (hydrogen solid solution). The composition of the last one depends on the amount of substituted nickel, and increases with increasing substituted cobalt. Thus Co-free alloys absorb smaller amount of hydrogen and form hydride with constant

hydrogen content (around 4 H/f.u.). The equilibrium plateau decreases under Ni/Co substitution, for example, it is 10 times smaller for $NdMgNi_2Co_2$ than for $NdMgNi_4$, but in both cases these equilibrium pressure are inside the electrochemical window, except for the right part of curves of the PCT diagram of $NdMgNi_2Co_2$, which is above 1 bar. This is explained by a slight change in the electrochemical capacity of the electrodes (~250 mAh/g) based on all cobalt-substituted alloys compared to the gas capacity. Practically, the best electrochemical parameters can be obtained for the electrodes based on the alloys with low cobalt content ($y = 0.3\ldots 0.5$).

A slightly different character is observed in alloys where there is a R/Mg substitution. In alloys with low magnesium content, the equilibrium plateau falls below 0.01 bar, which is expected to lead to decrease the discharge capacity (up to 160 mAh/g). As the magnesium content increases, the pressure of the equilibrium plateau increases, but remains in the electrochemical window and the discharge capacity increases. Its growth is due to the lowering of the weight factor of the alloys as well as the larger amount of hydrogen involved in the electrochemical processes. As it was shown latter, this amount of hydrogen can be increased by additional Ni/Co substitution. Thus, performing double substitution of R/Mg and Ni/Co allows obtaining much higher reversible electrochemical capacity compared to classical $RMgNi_4$ alloys.

4. Conclusion

In this paper, the effect of combined Pr/Nd/Mg and Ni/Co substitutions in the $(Pr, Nd)_{2-x}Mg_xNi_{4-y}Co_y$ alloys on the phase structure, solid-gas hydrogenation properties and electrochemical performances were investigated in order to find the most interesting material for electrochemical application. The new $(R',R'')_{2-x}Mg_xNi_{4-y}Co_y$ (R', R'' = Pr, Nd; x = 0.8–1.2; y = 0–3) alloys crystallize in the MgCu4Sn-type structure. The alloys absorb hydrogen relatively easily forming the hydrides with preserved parent cubic structure with the exception of two orthorhombic representatives ($Pr_{0.5}Nd_{0.5}MgNi_4H_4$ and $Nd_{1.2}Mg_{0.8}Ni_4H_{4.8}$). Twelve first hydrogenation curves were presented and analyzed by using the Johnson-Mehl-Avrami equation. Thermodynamic properties for the $Nd_{1.2}Mg_{0.8}Ni_3Co$ and $Nd_{0.8}Mg_{1.2}Ni_3Co$ hydrides were studied by PCT measurements. Cyclic stability has been measured at a charge-discharge current density of 50 mA/g (x = 0.8–1.2) and 200 mA/h (x = 1.0). Electrode materials with x = 1.2 are characterized by improved performance due to both weight lowering and enhanced H capacity. There is almost no difference between Pr or Nd substitution. The Co for Ni substitution in the alloy leads to significant increase of discharge capacities but lower cyclic stability. Maximum capacity is clearly observed within row: $Pr_{0.4}Nd_{0.4}Mg_{1.2}Ni_4$ (262 mAh/g) - $Pr_{0.4}Nd_{0.4}Mg_{1.2}Ni_{3.5}Co_{0.5}$ (276 mAh/g) - $Pr_{0.4}Nd_{0.4}Mg_{1.2}Ni_3Co$ (293 mAh/g) - $Pr_{0.4}Nd_{0.4}Mg_{1.2}Ni_2Co_2$ (309 mAh/g).

Acknowledgements This work was done in the frame of Ukraine and France Joint Project (Dnipro No. 2697YJ).

References:

[1] Yartys V.A., Ryabov O.B., Lototskyy M.V. Material science and structural chemistry of intermetallic hydrides. - Lviv: SPOLOM, 2006. - 288 p.

[2] Darren P. Broom. Hydrogen Storage Materials. The characterization of their storage properties // Springer, 2011. - 272 p.

[3] Linden D., Reddy T.B. Handbook of batteries, 3rd ed. // The McGraw-Hill Companies. Inc, 2002. - 1453 p.

[4] Sakintuna B., Lamari-Darkrim F., Hirscher M. Metal hydride materials for solid hydrogen storage: A review // Int. J. Hydrogen Energy, 2007 Vol. 32. P. 1121-1140.

[5] Verbovytskyy Yu.V., Zavaliy I.Yu. New metal-hydride electrode materials based on $R_{1-x}Mg_xNi_{3-4}$ alloys for chemical current sources // Materials science 51(4) (2016) 443-456.

[6] Villars P., Cenzual K. (Eds.), Pearson's Crystal Data - Crystal Structure Database for Inorganic Compounds, Release 2014/15, ASM International, Materials Park, OH, 2014.

[7] Verbovytskyy Yu.V., Zavaliy I.Yu. New metal-hydride electrode materials based on $R_{2-x}Mg_xNi_4$ alloys for chemical current sources // Materials science 52(6) (2017) 747-759.

[8] Wang Z.M., Zhou H.Y., Cheng G., Gu Z.F., Yu A.B. Preparation and electrode properties of new ternary alloys: $REMgNi_4$ (RE = La, Ce, Pr, Nd) // J. Alloys Compd. 384 (2004) 279-282.

[9] Liu Y., Cao Y., Huang L., Gao M., Pan H. Rare earth-Mg-Ni-based hydrogen storage alloys as negative electrode materials for Ni/MH batteries // J. Alloys Compd. 509(3) (2011) 675-686.

[10] Guéneé L., Favre-Nicolin V., Yvon K. Synthesis, crystal structure and hydrogenation properties of the ternary compounds $LaNi_4Mg$ and $NdNi_4Mg$ // J. Alloys Compd. 348 (2003) 129-137.

[11] Chotard J., Sheptyakov D., and Yvon K. Hydrogen induced site depopulation in the $LaMgNi_4$-hydrogen system // Z. Kristallogr. 223 (2008) 690-696.

[12] Sakaki K., Terashita N., Tsunokake S., Nakamura Y., Akiba E. In situ X-ray diffraction study of phase transformation of $Mg_{2-x}Pr_xNi_4$ during hydrogenation and dehydrogenation (x = 0.6 and 1.0) // J. Phys. Chem. C. 116 (2012) 1401-1407.

[13] Sakaki K., Terashita N., Tsunokake S., Nakamura Y., Akiba E. Effect of rare earth elements and alloy composition on hydrogenation properties and crystal structures of hydrides in $Mg_{2-x}RE_xNi_4$ // J. Phys. Chem. C. 116 (2012) 19156-19163.

[14] Terashita N., Sakaki K., Tsunokake S., Nakamura Y., Akiba E. Hydrogenation properties of ternary intermetallic compounds $Mg_{2-x}Pr_xNi_4$ // Mat. Trans. 53 (2012) 513-517.

[15] Denys R.V., Riabov A.B., Černý R., Koval'chuk I.V., Zavaliy I.Yu. New $CeMgCo_4$ and Ce_2MgCo_9 compounds: Hydrogenation properties and crystal structure of hydrides // J. Solid St. Chem. 187 (2012) 1-6.

[16] Sakaki K., Terashita N., Kim H., Proffen T., Majzoub E.H., Tsunokake S., Nakamura Y., Akiba E. Crystal structure and local structure of $Mg_{2-x}Pr_xNi_4$ (x = 0.6 and 1.0) deuteride using in situ neutron total scattering // Inorg. Chem. 52(12) (2013) 7010-7019.

[17] Shtender V.V., Denys R.V., Paul-Boncour V., Riabov A.B., Zavaliy I.Yu. Hydrogenation properties and crystal structure of $YMgT_4$ (T = Co, Ni, Cu) compounds // J. Alloys Compd. 603 (2014) 7−13.

[18] Czub J., Shtender V.V., Przewoźnik J., Zarzeska A., Hoser A., Gondek Ł. On the properties of the novel $CeMgNi_2T_2$ (T = Co, Cu) alloys and their hydrides // J. Alloys Compd. 814 (2020) 152244 (1-7).

[19] Verbovytskyy Yu.V., Shtender V.V., Lyutyy P.Ya., Zavaliy I.Yu., Electrode materials based on $LaMgNi_{4-x}Co_x$ ($0 < x < 1$) alloys // Powder Met. Met. Ceramics 55(10-11) (2017) 559-566.

[20] Verbovytskyy Yu.V., Shtender V.V., Hackemer A., Drulis H., Zavaliy I.Yu., Lyutyy P.Ya., Solid-gas and electrochemical hydrogenation properties of the $La_{1-x}Nd_xMgNi_{4-y}Co_y$ alloys // J. Alloys Compd. 741 (2018) 307−314.

[21] Oprysk V.O., Verbovytskyy Yu.V., Shtender V.V., Lyutyy P.Ya., Zavaliy I.Yu., The $Pr_{1-x}La_xMgNi_{4-y}Co_y$ alloys: Synthesis, structure and hydrogenation properties // Solid State Sciences. (2018). - Vol. 84. - P. 112-119.

[22] Shtender V.V., Denys R.V., Paul-Boncour V., Verbovytskyy Yu.V., Zavaliy I.Yu. Effect of Co substitution on hydrogenation and magnetic properties of $NdMgNi_4$ alloy // J. Alloys Compd. 639 (2015) 526−532.

[23] Shtender V.V., Paul-Boncour V., Denys R.V., Crivello J.-C., Zavaliy I.Yu. $TbMgNi_{4-x}Co_x$−$(H,D)_2$ system. I: Synthesis, hydrogenation properties, and crystal and electronic structures // J. Phys. Chem. C 124(1) (2020) 196-204.

[24] Verbovytskyy Yu.V., Zavaliy I.Yu., Berezovets V.V., Lyutyy P.Ya. Solid gas and electrochemical hydrogenation properties of the $R_{1-x}R'_xMgNi_{4-y}Co_y$ (R, R' = Y, La, Ce) alloys // Phys. Chem. Solid State 21(3) (2020) 503-509.

[25] Verbovytskyy Yu., Kosarchyn Yu., Zavaliy I. Solid gas and electrochemical hydrogenation properties of the selected $R,R'MgNi_{4-x}M_x$ (R,R' = La, Pr, Nd; M = Fe, Mn; x = 0.5, 1) alloys // French-Ukrainian J. Chem. 8(2) (2020) 126-139.

[26] Kraus W., Nolge G. PowderCell for Windows. Version 2.3. - Federal Institute for Materials Research and Testing. Berlin, Germany, 1999.

[27] Rodriguez-Carvajal J., Roisnel T. FullProf.98 and WinPLOTR: New Windows 95/NT Applications for Diffraction Commission for Powder Diffraction, International Union for Crystallography, Summer, 1998. Newsletter N20 (May-August).

[28] Akselrud L., Grin Yu. WinCSD: software package for crystallographic calculations (Version 4) // J. Appl. Crystallogr. 47 (2014) 803-805.

[29] Sato T., Mochizuki T., Ikeda K., Honda T., Otomo T., Sagayama H., Yang H., Luo W., Lombardo L., Zuttel A., Takagi S., Kono T., Orimo S.-i., Crystal structural investigations for understanding the hydrogen storage properties of $YMgNi_4$-based alloys // Acs Omega, 5 (2020) 31192-31198.